Kinetic Modeling of Cyclohexane Oxidation including PAH Formation

N. A. Slavinskaya*, M. Abbasi, U. Riedel

Institute of Combustion Technology, German Aerospace Center (DLR), Stuttgart

Abstract

This cyclohexane reaction sub-model for high and low temperature oxidation has been developed on the base of the DLR C_0-C_4 kinetic model with the PAH formation. The reaction model was successfully validated on the experimental data for ignition delay measured in rapid compressor machine and shock tube experiments, laminar flame speed data and the species concentration profiles measured in laminar flames at low and atmospheric pressure. The chemical pathways leading to the PAH formation are well understood. For temperatures lower than 1200K, the cyclohexane dehydrogenation is the dominant way to produce benzene. At higher temperatures, propargyl recombination is the dominant way.

Introduction

Cycloalkanes (naphthenes) are an important chemical class of hydrocarbons found in diesel, kerosene and gasoline, which affect the ignition quality of the fuel and raise soot emission levels, because they are known to dehydrogenate and produce aromatics, leading to the production of polycyclic aromatics and soot growth. The semi-detailed reaction model for cyclohexane combustion including formation of PAH (poly aromatic hydrocarbons), which are known as precursors of soot, has been developed to be included in reference fuel models.

This reaction mechanism has been developed for high and low temperature oxidation of cyclohexane on the base of the DLR C_0-C_4 kinetic model with the PAH formation sub-model [1,2]. During the cyclohexane mechanism development, the generic reactions for both regimes of the cyclo- hydrocarbon oxidation are determined. The actual uncertainty levels of main reaction rate coefficients have been calculated and empirical methods for evaluation of rate coefficients of several reaction types have been investigated as well. The high temperature oxidation proceeds through:

- unimolecular fuel decomposition;
- H-atom abstraction leading to cycloalkyl radical, cy-C_6H_{11};
- cy-C_6H_{11} β-scission decomposition, producing olefins and di-olefins;
- cascading dehydrogenation leading to benzene and smaller radicals;
- isomerisation and decomposition of linear hexenyl radicals after the ring-opening step.

The low temperature cyclohexane oxidation can be described with the general scheme for the low temperature oxidation of acyclic alkanes, but with the formation of intermediate species with 2 rings, specifically bi-cyclic ethers and cyclic ketones.

The low temperature oxidation proceeds through:

- cy-C6H11O• and cycloperoxy radical (cy-C6H11OO•) formation from reactions of cy-C6H11• with O2 and O•, leading to further chain branching pathways;
- isomerisation of cy-C6H11OO• to cyclohydroperoxy radicals (cy-C6H10OOH•) through the 4-, 5-, 6-, and 7- centre transition states;
- decomposition of cy-C6H10OOH• radicals to cyclohexanone, three bicyclic ethers and smaller species;
- decomposition of cy-C6H10OOH• radicals to linear hex-5-enal cyclohexene;
- O2 addition to cy-C6H10OOH• with formation of O2QOOH• type radicals;
- decomposition of O2QOOH• to cyclic ketohydroperoxides;
- decomposition of cyclic ketohydroperoxides OQOOH to hydroxyl radical and smaller species;
- decomposition of bicyclic ethers and cyclohexanone through the ring opening steps to small olefin molecules and ketone radicals, as well as the hex-5-enal molecule, which decomposes further to smaller species.

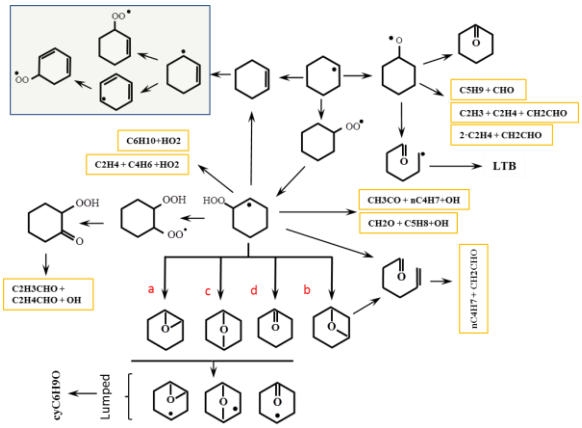

Figure 1 Principal scheme of the low temperature cy-C6H12 oxidation.

* Corresponding author: nadja.slavinskaya@dlr.de

The formation and subsequent dissociation of cyclic hydroperoxides marks an important difference in low temperature naphtene oxidation with respect to linear hydrocarbon reactions. This consequently leads to different steps and new decomposition paths, which have to be established and estimated in rate properties. This was done using different approaches, such as analogy with a similar reaction, analysing the strengths of the bonds in a molecule, or implementing empirical methods.

The principal scheme of the low-temperature reaction paths adopted in the model is presented in Fig.1. The grey block in Fig.1 was reduced in the developed mechanism.

The thermodynamic and transport data followed from [3,4] or have been evaluated with the Benson group additive method [5] and empirical method [6-10].

The behaviour of the high and low temperature cyclohexane oxidation model was validated and optimized on the simulation of ignition delay time over the temperature range of 600-1700K in various equivalence ratio and pressure ranges. Experimental data was obtained from rapid compression machines (RCM) [11,12] and shock tubes (ST) [13]. Laminar flame speed data [14] was obtained at standard room pressure and temperature, and PAH formation was observed in laminar premixed cyclohexane flames [15,16], Tab.1.

Table 1 Experimental data, used for validations.

	Validation		
	ST	RCM	Flame Structure
1			**Concentration profile** [15] T= 1000 K, p= 30 Torr, φ=1.0 CHX/O_2 in 32.5% Ar
2		**Ignition delay time [12]** T= 600-900 K φ = 1.0, p= 12.5, 20 bar CHX/air	
3		**Ignition delay time [11]** p= 8, 14 bar T= 650-900 K , φ=1.0 CHX/ air	
4			**Flame Speed [14]** T= 298 K p= 1atm, φ=0.8-1.6 CHX/ air
5	**Ignition delay time [13]** T= 1230-1840 K, p= ~ 8atm φ=0.5, 1.0, 2.0 CHX/O_2 /Ar		
6			**Concentration profile [16]** T_0= 700 K, p= 1 atm, φ=2.33 **Mixture**: CHX/O_2 in 39.4% N_2

Results and discussion

The simulation of experimental data for ignition delay times of [11-13] are shown in Fig. 2-4. The ignition delay times, measured in an RCM, have been defined in simulations as the time from the end of compression to the maximum rate of pressure rise due to ignition.

The results shown in Figures 2 and 3 illustrate that the model predicted ignition delay times measured in an RCM [11, 12] for both low and high temperature oxidation regimes well. The model reproduced the two stage ignition for all investigated pressures and stoichiometric ratios. The data [11] measured at a pressure of 0.8 MPa and 1.4 MPa, within the temperature range of 650-900 K, are very well reproduced by the model, Fig.2.

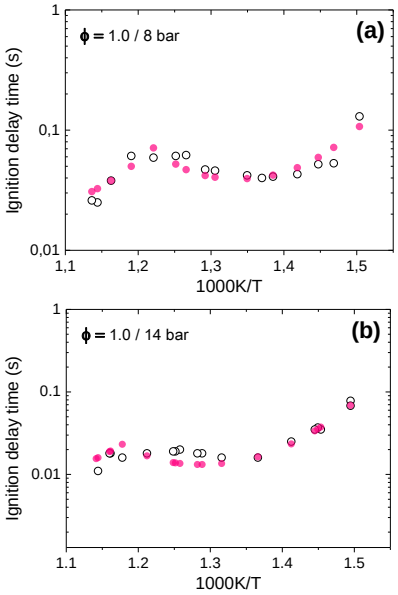

Figure 2 Cyclohexane ignition delay time from RCM experiments [11], for φ=1: a) p=8 bar, b) p=14 bar. Closed symbols-simulations; open -experimental data.

Data obtained in the study [12] at 20 bar are slightly under-predicted for middle temperature at φ=0.5, Fig.3b, and for low temperature at φ=1, Fig.3a.

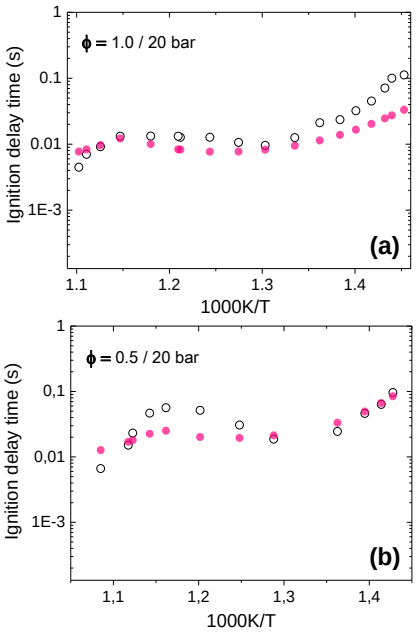

Figure 3 Cyclohexane ignition delay time from RCM experiments in 20 bar [12]; a) φ=1 b) φ=0.5 .Close symbols-simulations; open dots-experimental data.

The data of Sirjean et al. [13] for ignition delay times of cyclohexane–oxygen–argon were obtained in a shock tube for temperatures between 1230 - 1840 K and a pressure range of 0.73 – 0.95 MPa. These data are slightly under-predicted by the present mechanism at φ=0.5 and over-predicted at φ=2, Fig.4. The model demonstrates an excellent agreement with laminar flame speed data, Fig.5.

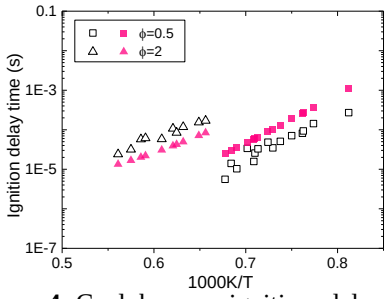

Figure 4 Cyclohexane ignition delay time from the shock-tube experiment [13] at φ=0.5 and 2. Close and open symbols represent simulation results and experimental data, respectively.

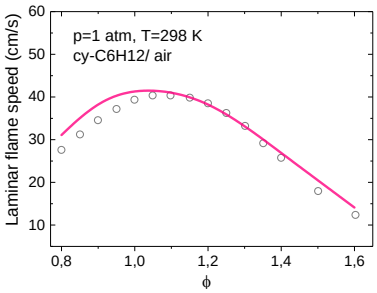

Figure 4 Cyclohexane laminar flame speed. The solid line- simulation; symbols- experimental data [14].

Results of the experimental data simulations, Figures 2-5, demonstrate that the model correctly reflects the cyC_6H_{12} oxidation and heat release. This allows the use of the developed mechanism for an investigation into the main steps of PAH and their precursor formation.

In this way, the species concentration profiles measured in atmospheric and low-pressure laminar flames [15,16] were simulated, Fig.6 and 7. All of the simulations were performed using the temperature profiles provided by the authors of [15,16].

Results of modeling the mole fraction profiles of the PAH precursors [15] at p= 30 Torr and **φ**=1.0 are shown in Fig.6. A good agreement with data [15] for the major products (CO_2, H_2, H_2O), Fig.6a-c, the most important PAH precursors, C_2H_2, C_3H_4, C_3H_3 and cyC_5H_6, Fig.6 d-f, j, and intermediates C_3H_6, nC_4H_7, and cyC_9H_{11} Fig.6 g,h,l, is achieved. Concentration of cyC_5H_5 and C_6H_6 (Or A1, benzene) is over- predicted by a factor of 2, Fig.6i,k. The measured profile of C_3H_6 is slightly under-predicted, while concentrations of C_3H_3, nC_4H_7, and cyC_5H_5 are slightly over-predicted. But the main disagreement for these species is observed to be the location of the concentration maximum of C_3H_6, cyC_5H_5 and cyC_5H_6, Fig.6g,I,j. The possible reason for this is the uncertainty of the temperature and location measurements.

Mole fractions of reactants (cyC_6H_{12}, O_2) and major products (CO, CO_2, H_2, CH_4 and C_2H_2) measured and simulated in the atmospheric flame [16] at **φ**=2.33 are shown in Fig.7a-d. The reaction mechanism reproduces the mole fraction profiles of each species well. However, concentrations of CH_4 and C_2H_2 are slightly under- predicted, Fig.7d. For the intermediate species C_2H_4, C_3H_4, C_3H_6, C_4H_4, and C_4H_6, the model predicts well both the experimental concentration values and maximum locations, Fig.7e,f,h,j.

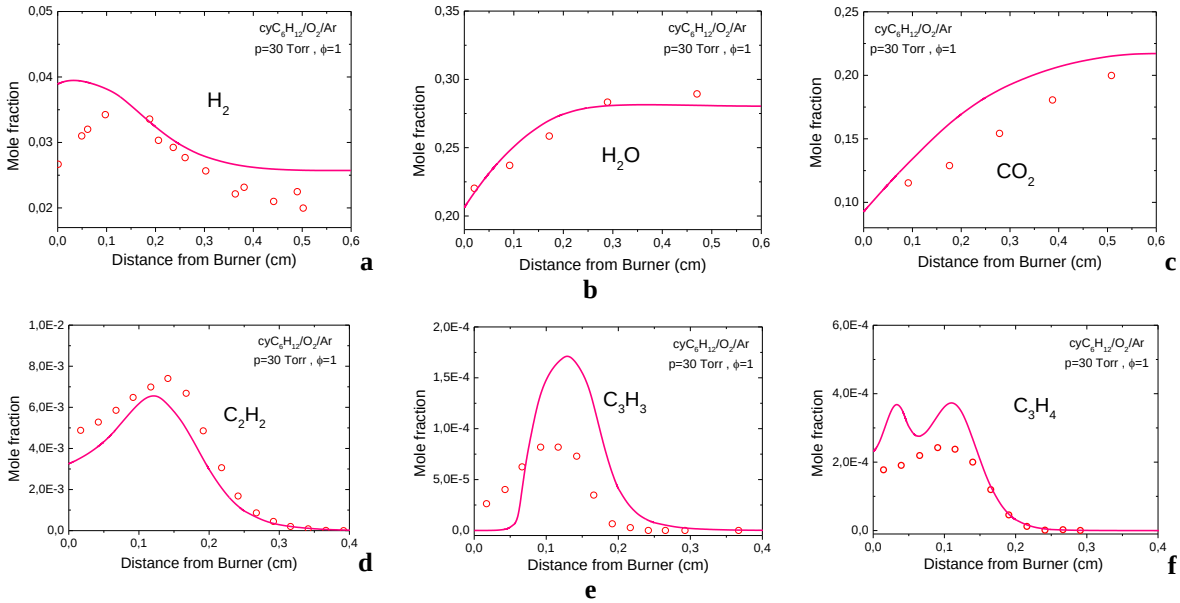

Figure 6 Simulated and experimental [15] concentration profiles of the soot precursors species. Symbols are experiments; solid lines-predicted profiles.

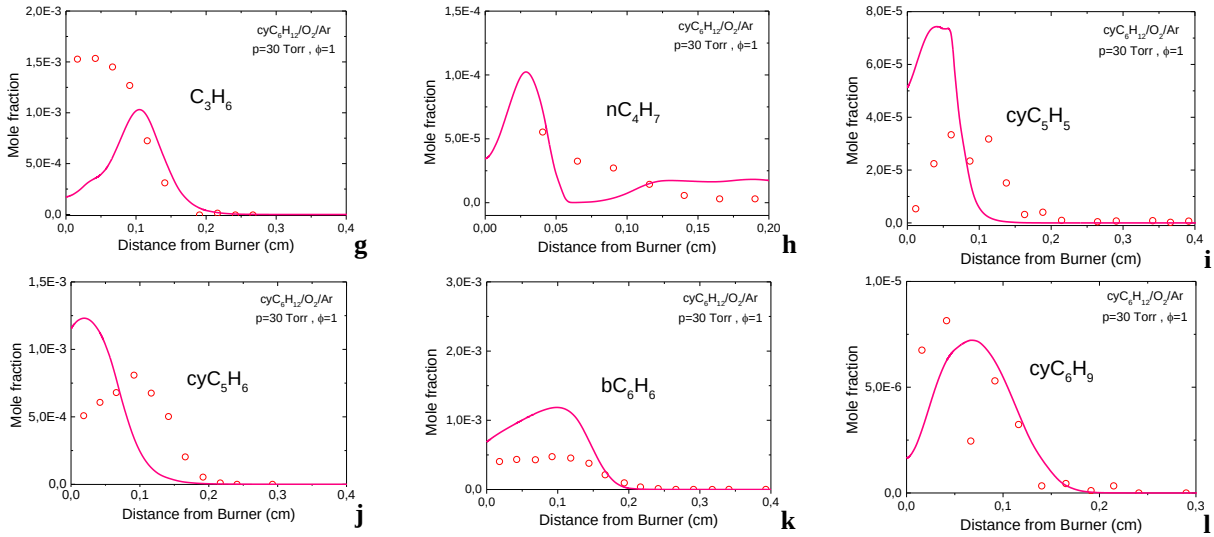

Figure 6 Simulated and experimental [15] concentration profiles of the soot precursors species. Symbols are experiments; solid lines-predicted profiles.

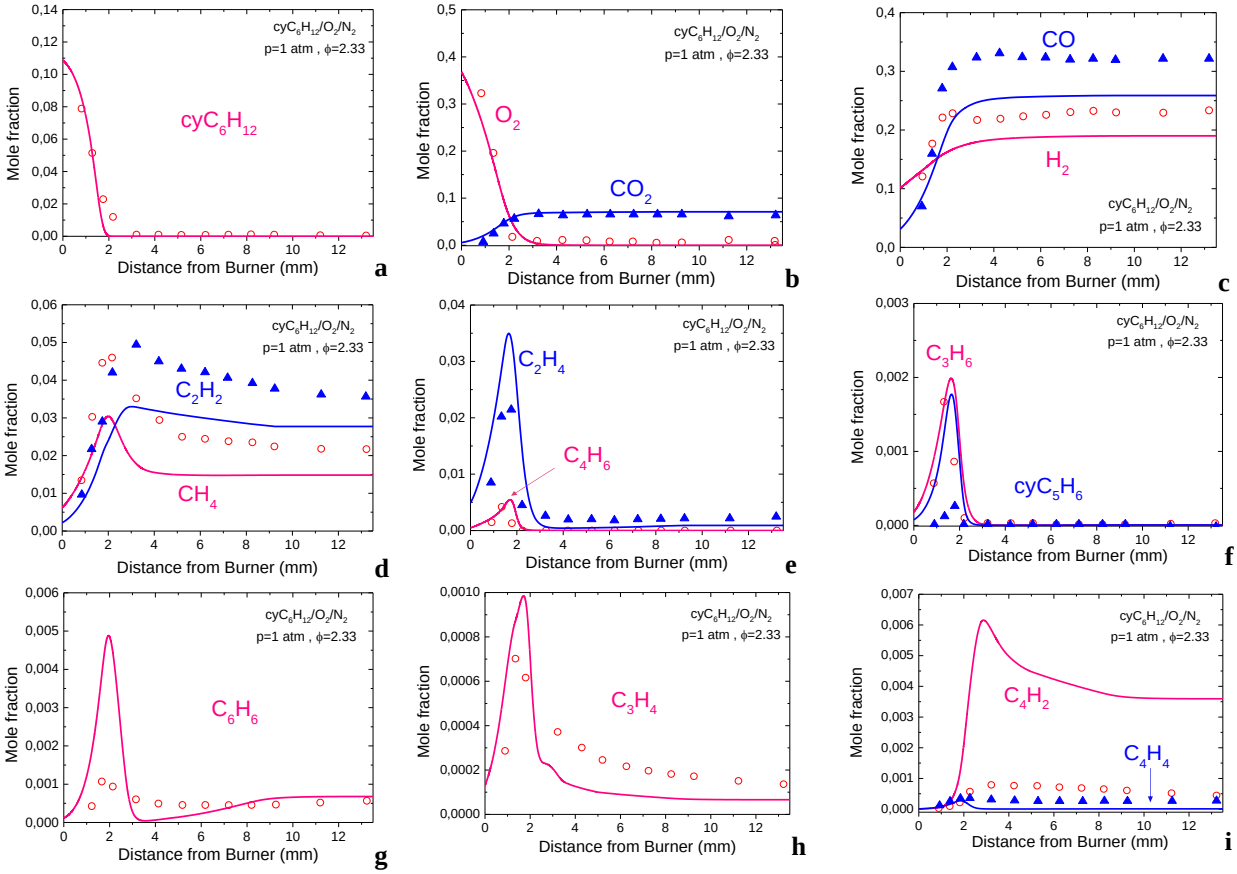

Figure 7. Species concentration profiles from the cyclohexane flame [16]. Symbols are experiments; solid lines-predicted profiles.

Simulated concentrations of cyC_5H_6 and C_4H_2 have the highest disagreement with experimental data by factors of 4 and 6, respectively. Benzene formation is also over-predicted at the concentration maximum, but is in excellent agreement with the observations in the post-flame zone, Fig.7g. The simulated data disagrees with experimental data [15,16] in the worst case by a factor 6.

The simulated concentration profiles of species important for aromatic molecule production, C_2H_2, C_3H_4 and C_3H_4, are in good agreement with experimental data, Fig.6,7.

For the PAH reaction path analysis, Fig.8, we used two simulations, at T≈ 900K and T=1460K, of data [16]. The PAH formation goes through two parallel channels; formation of benzene via direct

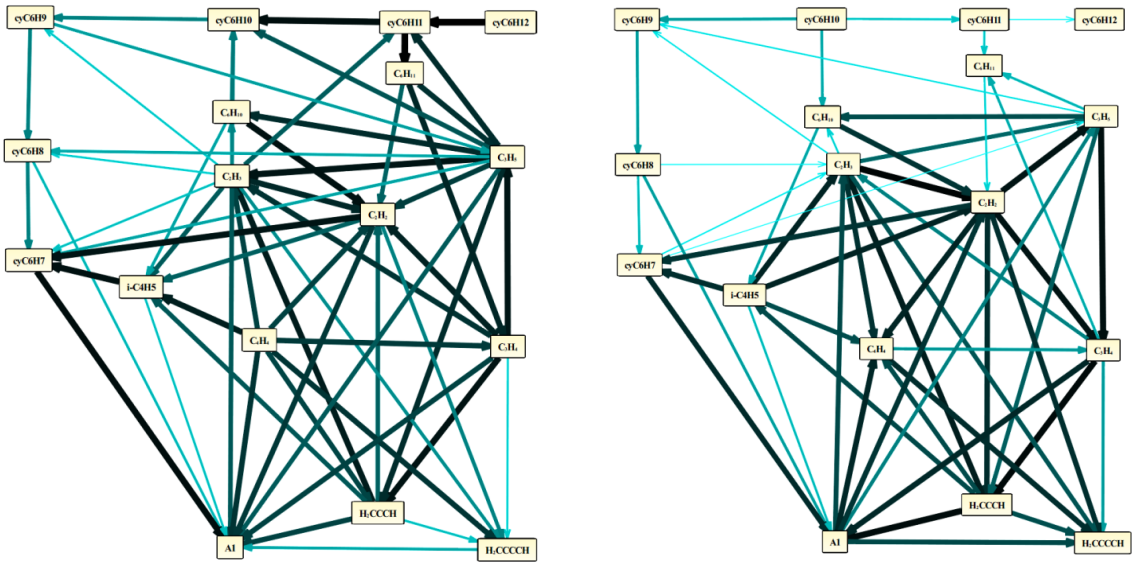

(a) H=0.065 cm, T=896 K (b) H= 0.209 cm, T=1460 K

Figure 8 Reaction flux diagram of PAH formation in cyC_6H_{12}/air flame. T_0= 700 K, p= 1 atm, φ=2.33.

dehydrogenation of the cyclohexane and from reactions of C_3H_x and C_4H_x molecules and radicals.

The modeling results showed clear temperature dependence of dominating reaction routes leading to aromatics. In the low temperature regime, 700K < T < 1200 K, Fig.8, benzene production is dominated by the dehydrogenation of cyclohexane. For temperatures T >1200 K, reactions of C_3H_3 and C_3H_4 become more important. The large PAH molecules are produced through the HACA mechanism, reactions between aromatic molecules/radicals and small molecules, and reactions between aromatic molecules and aromatic radicals.

Conclusion

A skeletal reaction mechanism for low and high temperature cyclohexane oxidation with PAH formation is reported. This mechanism is an extension of the DLR hydrocarbon reaction database with the cycloalkane oxidation sub-model.

The reaction model was successfully validated on the experimental data for ignition delay measured in rapid compressor machine and shock tube experiments, laminar flame speed data and the species concentration profiles measured in laminar flames at low and atmospheric pressure.

An important feature of this mechanism is its ability to predict the formation of benzene and PAH growth. The chemical pathways leading to their formation are well understood. It has been shown that both reaction paths to benzene, via dehydrogenation of cyclohexane and via recombination of small radicals, are equally important. For temperatures lower than 1200K, the cyclohexane dehydrogenation is the dominant way to produce benzene. At higher temperatures, propargyl recombination is the dominant way. The formation of large aromatic molecules can proceed from small radicals, parallel with the dehydrogenation of cyclohexane.

References

1. N.A. Slavinskaya, P. Frank, Combust. Flame, 156 (2009) 1705-1722.
2. V. Chernov, M. J.Thomson, S. B., N. A. Slavinskaya, U. Riedel, Combust. Flame 161 (2014) 592–601.
3. W.H. Green, J.W. Allen, R.W. Ashcraft, G.J. Beran, C.A. Class, C. Gao, C.F. Goldsmith, M.R. Harper, A. Jalan, G.R. Magoon, D.M. Matheu, S.S. Merchant, J.D. Mo, S. Petway, S. Raman, S. Sharma, J. Song, K.M. Van Geem, J. Wen, R.H. West, A. Wong, H.W. Wong, P.E. Yelvington, J. Yu, Thermo Data Estimator; RMG v. 3.3.0, 2011.
4. E. Goos, A. Burcat, B. Ruscic, Ideal Gas Thermochemical Database with updates from Active Thermochemical Tables; <ftp://ftp.technion.ac.il/pub/supported/aetdd/thermodynamics>; 03/28/2012. ; mirrored at <http://garfield.chem.elte.hu/Burcat/burcat.html>; 11/13/2014.
5. S.W. Benson, F. R. Cruickshank, D. M. Golden, G. R. Haugen, H. E. O'Neal, A. S. Rodgers, R. Shaw, R. WALSH, Additivity rules for the estimation of thermochemical properties, Department of Thermochemistry and Chemical Kinetics, Stanford Research Institute, Menlo Park, California 94025, April 1968.
6. K.G. Joback, R.R. Reid, Chem. Eng. Comm. 1987, vo157, pp. 233-243.
7. Dixon-Lewis, G., "Flame structure and flame reaction kinetics. II. Transport phenomena in multi-component systems", Proceedings of the Royal Society A. 304, pp. 111-135 .1968.
8. J.Warnatz, "Numerical Methods in Flame Propagation", edited by N. Peters and J. Warnatz. Vieweg and Sohn, Wiesbaden, 1982.

9. R.J. Kee, J. Warnatz, J.A. Miller, "A Fortran Computer Code Package for the Evaluation of Gas-Phase Viscosities, Conductivities, and Diffusion Coefficients", Sandia National Laboratories Report SAND83-8209, 1983.

10. R.J. Kee, G. Dixon-Lewis, J. Warnatz, M.E. Coltrin, J.A. Miller, A Fortran Computer Code Package for the Evaluation of Gas-Phase Multicomponent Transport Properties, Report SAND86-8246, 1986.
11. O. Lemaire, M. Ribaucour, M. Carlier, R. Minetti, Combust. Flame 127 (2001) 1971.

12. S. Vranckx, C. Lee, H.K. Chakravarty, R.X. Fernandes, Proc. Combust. Inst. 34 (2012) 377–384.
13. B. Sirjean, F. Buda, H. Hakka, P.A. Glaude, R. Fournet, V. Warth, F. Battin-Leclerc, M.R. Lopez, Proc. Combust. Inst. 31 (2007) 277–284.
14. S.G. Davis, C.K. Law, Combust. Sci. Tech. 140 (1998) 427-449.
15. M. E. Law, P. R Westmoreland, T. A. Cool, J. Wang, N. Hansen, T. Kasper, Proc. Combust. Inst. 2007, 31, 565.
16. A. Ciajolo, A.Tergrossi, M.Mallardo, T.Faravelli, E.Ranzi, Proc. Combust. Inst. 32 (2009) 585-591.